*Inorg. Chem.* **2007**, *46*, 501–509


# Electron-Sponge Behavior and Electronic Structures in Cobalt-Centered Pentagonal Prismatic $Co_{11}Te_7(CO)_{10}$ and $Co_{11}Te_5(CO)_{15}$ Cluster Anions

**Olivier Cador,[§] Hélène Cattey,[‡] Jean-François Halet,[§] Walter Meier,[†] Yves Mugnier,[‡] Joachim Wachter,*[,†] Jean-Yves Saillard,[§] Bachir Zouchoune,[§,⊥] and Manfred Zabel[†]**

*Institut für Anorganische Chemie, Universität Regensburg, D-93040 Regensburg, Germany, Laboratoire de Synthèse et Electrosynthèse Organométalliques (UMR-CNRS 5188), Faculté des Sciences Mirande-9, Allée Alain Savary, Université de Bourgogne, F-21000 Dijon, France, Sciences Chimiques de Rennes (UMR-CNRS 6226), Université de Rennes I, F-35042 Rennes Cedex, France, and Laboratoire de Chimie Moléculaire, du Contrôle de l'Environnement et des Mesures Physico-chimiques, Université Mentouri-Constantine, 25000 Constantine, Algeria*

Received October 5, 2006

The novel cluster anion $[Co_{11}Te_5(CO)_{15}]^-$ (**[3]**$^-$) has been isolated and structurally characterized as part of the salt $[Cp^*_2Nb(CO)_2]$**[3]** ($Cp^* = C_5Me_5$). The cobalt-centered $Co_{10}$ pentagonal prism is surrounded by a shell of two $\mu_5$-Te, three $\mu_4$-Te ligands, and 15 CO groups in terminal, symmetrical, and $\sigma$-semibridging bonding modes. The hybrid carbonyl-telluride character of the ligand shell is reflected in the solid state by a one-dimensional assembly of polyhedral prisms along a backbone of $[Cp^*_2Nb(CO)_2]^+$ cations. Electrochemical studies reveal the presence of four redox couples of **[3]**$^n$ ($n = -1$ to $-5$). The electronic structures of various metal-centered and empty pentagonal-prismatic (PP) $M_{10}$ clusters (M = Co, Ni) are calculated and compared to those of pentagonal-antiprismatic (PA) $M_{10}$ structures. Closed-shells of 152 and 156 metal valence electrons, respectively, are found to determine the electronic structures and chemical properties of these geometries. From these considerations, magnetic properties have been predicted. They have been verified for the $[Co_{11}Te_7(CO)_{10}]^-$ cluster anion, which exhibits a singlet–triplet gap of 0.318 kcal/mol.

## Introduction

Transition metal clusters are at the interface between molecular and solid-state chemistry. Apart from synthetic efforts, the design of materials with new properties, such as molecular capacitors or molecular magnets, has become an attractive goal. An important target for such investigations are highly connected and symmetric transition metal carbonyl clusters bearing a protecting shell of CO or main group ligands.[1] The interest in investigating such compounds is based on their potential to exhibit several electrochemically reversible or quasi-reversible redox systems without structural rearrangement of the cluster skeleton.[2,3]

We have recently reported on the electron-sponge behavior of the $[Co_{11}Te_7(CO)_{10}]^{1-,2-}$ (**[1]**$^{1-,2-}$) cluster anions.[4,5] These cluster anions belong to the rare class of pentagonal prismatic (PP) metal clusters[6] in which the metal skeleton is surrounded by a shell of carbonyl and main group ligands (Figure 1).[7] An additional metal atom lies in the interstitial cavity. Empty

* To whom correspondence should be addressed. E-mail: joachim.wachter@chemie.uni-regensburg.de. Fax: (+49) 941-943-4439.
† Universität Regensburg.
‡ Université de Bourgogne.
§ Université de Rennes I.
⊥ Université Mentouri-Constantine.

(1) Longoni, G.; Femoni, C.; Iapalucci, M. C.; Zanello, P. In *Metal Clusters in Chemistry*, Vol. 3; Braunstein, P., Oro, L. A., Raithby, P. R., Eds.; Wiley-VCH: Weinheim, Germany, 1999; pp 1137−1158.
(2) Femoni, C.; Iapalucci, M. C.; Longoni, G.; Svensson, P. H. *Chem. Commun.* **2004**, 2274−2275.
(3) (a) Lewis, G. J.; Roth, J. D.; Montag, R. A.; Safford, L. K.; Gao, X.; Chang, S.-C.; Dahl, L. F.; Weaver, M. J. *J. Am. Chem. Soc.* **1990**, *112*, 2831−2832. (b) Roth, J. D.; Lewis, G.; Safford, L. K.; Jiang, X.; Dahl, L. F.; Weaver, M. J. *J. Am. Chem. Soc.* **1992**, *114*, 6159−6169.
(4) Brunner, H.; Lucas, D.; Monzon, T.; Mugnier, Y.; Nuber, B.; Stubenhofer, B.; Stückl, A. C.; Wachter, J.; Wanninger, R.; Zabel, M. *Chem.—Eur. J.* **2000**, *6*, 493−530.
(5) Brunner, H.; Cattey, H.; Meier, W.; Mugnier, Y.; Stückl, A. C.; Wachter, J.; Wanninger, R.; Zabel, M. *Chem.—Eur. J.* **2003**, *9*, 3796−3802.
(6) Seidel, R.; Kliss, R.; Weissgräber, S.; Henkel, G. *J. Chem. Soc., Chem. Commun.* **1994**, 2791−2792.
(7) MacGillivray, L. R.; Atwood, J. L. *Angew. Chem., Int. Ed.* **1999**, *38*, 1018−1033.

10.1021/ic061904+ CCC: $37.00 
Published on Web 12/20/2006

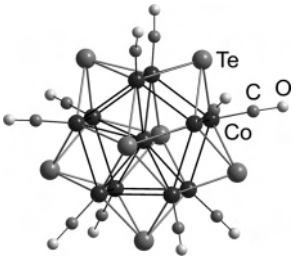


**Figure 1.** Structure of $[Co_{11}Te_7(CO)_{10}]^n$ ([**1**]$^n$; $n = -1$[4] and $-2$[7]), viewed down the pseudo-$C_5$ axis.

PP $M_{10}$ clusters are also known, for example, $[Ni_{10}(PMe)_7(CO)_{10}]^{2-}$.[8]

In continuation of our work, we wish to report on the novel anionic hybrid carbonyl-telluride cobalt clusters $[Co_{11}Te_5(CO)_{15}]^{1-,2-}$ ([**3**]$^{1-,2-}$) and their electrochemical reduction. The considerable electron-consuming capacities of the central $Co_{11}$ polyhedron prompted us to carry out DFT calculations of both pentagonal-prismatic $Co_{11}Te_7(CO)_{10}$ and $Co_{11}Te_5(CO)_{15}$ species. The flexibility of the electron counts has been confirmed, and first attempts are reported on a correlation of electronic structures and magnetic properties. For the purpose of comparison, an extension of the calculations for structurally related pentagonal antiprismatic (PA) $M_{10}$ and $M_{11}$ clusters were carried out.

## Results and Discussion

**Synthesis and Characterization.** We have recently shown that the reaction of $Cp^*_2Nb(Te_2H)$ ($Cp^* = C_5Me_5$) with $Co_2(CO)_8$ in boiling toluene (Scheme 1) gives a complex mixture of salts containing the cluster anions $[Co_{11}Te_7(CO)_{10}]^{1-,2-}$ ([**1**]$^{1-,2-}$) and $[Co_9Te_6(CO)_8]^{1-,2-}$ ([**2**]$^{1-,2-}$). These were identified crystallographically either after crystallization directly from the reaction mixture or after column chromatography on silica gel.[4,9] The appropriate cation $[Cp^*_2Nb(CO)_2]^+$ has formed by back transfer of CO from $Co_2(CO)_8$ as part of the global ligand-cross-transfer in this reaction.[10]

A reinvestigation of the reaction taking care of the existence of still more polar compounds led to the isolation of $[Cp^*_2Nb(CO)_2]$**[3]** in a 6% yield containing the novel cluster anion $[Co_{11}Te_5(CO)_{15}]^-$ ([**3**]$^-$) (Scheme 1). Its composition has been confirmed by elemental analysis, mass spectrometry, and X-ray diffraction analysis. The positive-ion electrospray ionization mass spectrometry (PI-ESI-MS) shows a peak at $m/z = 419$ corresponding to the $[Cp^*_2Nb(CO)_2]^+$ cation. The negative (NI-ESI-MS) spectrum of $[Cp^*_2Nb(CO)_2]$**[3]** reveals an intense peak with center of gravity at $m/z = 1708$ ([**3**]$^-$) and another peak at $m/z = 853.6$ ([**3**]$^{2-}$). The relative intensities of both peaks depend on the applied energy. Loss of CO groups from the cluster core was not observed. IR spectra (KBr) exhibit strong $\nu$(CO) absorptions at 2007 ($[Cp^*_2Nb(CO)_2]^+$) and 1961 cm$^{-1}$. The latter is relatively broad and may be assigned to terminal $\nu$(CO) frequencies of the cation and the cluster anion. A less intense absorption at 1820 cm$^{-1}$ and a shoulder at 1790 cm$^{-1}$ are diagnostic with respect to the presence of two different kinds of bridging CO ligands (see below).

Crystals of $[Cp^*_2Nb(CO)_2]$**[3]** were obtained at $-20$ °C as dark needles from 10:1 $CH_2Cl_2$/acetone. The crystal structure consists of four molecular units in the orthorhombic cell, and each molecular unit contains one pair of $[Cp^*_2Nb(CO)_2]^+$ and $[Co_{11}Te_5(CO)_{15}]^-$ ions. The structure of the cation is typical of a bent peralkylated niobocene fragment bearing two CO ligands in a pseudotetrahedral geometry.[4]

The central feature of the cluster anion is, as in $[Co_{11}Te_7(CO)_{10}]^{1,2-}$ ([**1**]$^{1-,2-}$), a cobalt-centered pentagonal $Co_{10}$ prism (Figure 2) with the pentagonal faces of the prism being capped by two $\mu_5$-Te ligands. However, only three of the square faces are bridged by $\mu_4$-Te ligands. The other two faces are bridged by seven CO groups in two different bonding modes. The remaining eight CO groups are clearly of terminal character. Three symmetric bridges [C(4)−O(4), C(6)−O(6), and C(8)−O(8)] with mean Co−C bond lengths of 1.94(2) Å and Co−C−O angles of 139.7 (2)° are observed, linking together both pentagonal faces. The CO-bridged Co−Co distances are slightly shorter (between 0.05 and 0.14 Å) than the Co(2)−Co(2a) and Co(3)−Co(3a) distances. Symmetric CO bridges exist in $[Co_4(CO)_{10}(\mu_4\text{-}E)_2]$ (E = S,[11] Te,[11] PPh,[12] AsPh[13]) complexes, in which two opposite Co−Co bonds within the $Co_4$ rectangle are bridged. The CO ligands around Co(5) and Co(5a), which are oriented toward Co(4) and Co(6), respectively, exhibit bent semibridging character with significant Co−C $\sigma$-bond contribution.[14] This follows from Co−C−O angles in the range between 154.1(10) [Co(5)−C(7)−O(7)] and 167.4(12)° [Co(5)−C(5)−O(5)] and Co−C distances between 1.737 and 2.631 Å (Table 1).

Compared to the structure of the $[Co_{11}Te_7(CO)_{10}]^-$ anion, a distortion of the cobalt cage of [**3**]$^-$ is found which is expressed by Co−Co distances between 2.459(2) [Co(4)−Co(4a)] and 2.705(2) Å [Co(3)−Co(4)]. It is not clear how the deformation of the cobalt skeleton in **[3]**$^-$ is affected by the bridging CO groups and the increased number of $\pi$-acceptor ligands. The alternating intrapentagonal Co−Co bond lengths are particularly striking(Table 1). In contrast, the prismatic skeleton of **[1]**$^-$ is composed of five nearly perfect $Co_5Te$ octahedra [$d$(Co−Co) = 2.522(4)−2.612(4) Å]. As in **[1]**$^-$, the distances Co(1)−Te(1) [$d$ = 2.626(1) Å] are much shorter than the $\mu_4$-Te−Co(1) distances [mean of 3.481(2) Å] indicating an important compression along the pseudo-fivefold axis Te(1)−Co(1)−Te(1a).

The replacement of two Te ligands by five CO groups results in an increase in metal valence electrons (MVE)[18b] from 148 in [**1**]$^-$ to 150 MVE's in **[3]**$^-$. For the crystallographic data of clusters with the $Co_{11}$ core, it has been

(8) Rieck, D. F.; Gavney, J. A., Jr.; Norman, R. L.; Hayashi, R. K.; Dahl, L. F. *J. Am. Chem. Soc.* **1992**, *114*, 10369−10379.
(9) Meier, W.; Wachter, J. Unpublished results.
(10) Wachter, J. *Eur. J. Inorg. Chem.* **2004**, 1367−1378.
(11) Ryan, R. C.; Dahl, L. F. *J. Am. Chem. Soc.* **1975**, *97*, 6904−6906.
(12) Richmond, M. G.; Kochi, J. K. *Inorg. Chem.* **1986**, *25*, 1334−1345.
(13) DeSilva, R. M.; Mays, M. J.; Davies, J. E.; Raithby, P. R.; Rennie, M. A.; Shield, G. P. *J. Chem. Soc., Dalton Trans.* **1998**, 439−446.
(14) (a) Klingler, R. J.; Butler, W. M.; Curtis, M. D. *J. Am. Chem. Soc.* **1978**, *100*, 5034−5039. (b) Crabtree, R. H.; Lavin, M. *Inorg. Chem.* **1986**, *25*, 805−812.

**Scheme 1.** Summary of Cluster Anions Obtained from the Reaction of $Cp^*_2Nb(Te_2H)$ with $Co_2(CO)_8$[a]

$$Cp^*_2Nb(Te_2H) + Co_2(CO)_8 \xrightarrow[110\ ^\circ C]{\text{toluene}} [Co_{11}Te_7(CO)_{10}]^{1-,2-} + [Co_9Te_6(CO)_8]^{1-,2-} + [Co_{11}Te_5(CO)_{15}]^{1-,2-}$$

$$[\mathbf{1}]^{1-,2-} \qquad [\mathbf{2}]^{1-,2-} \qquad [\mathbf{3}]^{1-,2-}$$

[a] The cation is in all cases $[Cp^*_2Nb(CO)_2]^+$.

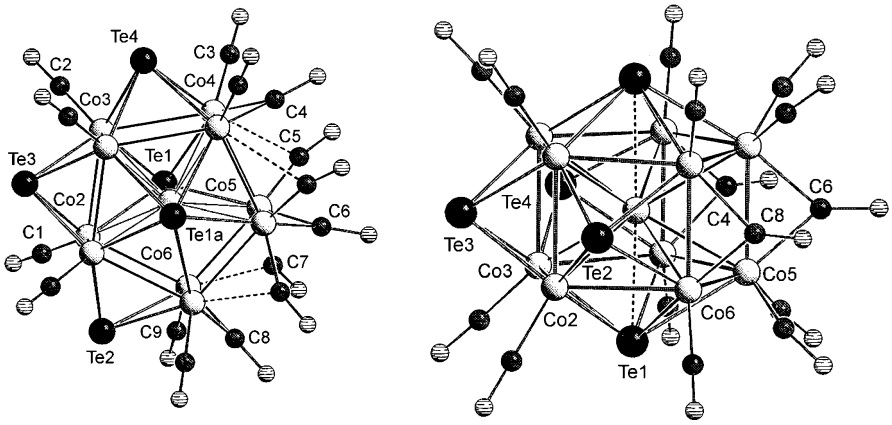


**Figure 2.** Molecular structure of the anion $[\mathbf{3}]^-$: (left) view along the axis Te(1)−$Co_{centr}$−Te(1a) [$Co_{centr}$ = Co(1)] and (right) side view, which rationalizes the symmetry plane through Co(1), Te(2), Te(3), Te(4), C(4), C(6), and C(8).

**Table 1.** Selected Distances (Å) and Angles (deg) for $[(C_5Me_5)_2Nb(CO)_2][\mathbf{3}$

| | | | |
|---|---|---|---|
| Te(1)−Co(1) | 2.626(1) | Co(2)−Co(6) | 2.698(2) |
| Te(1)−Co(2) | 2.533(2) | Co(3)−Co(3a) | 2.578(2) |
| Te(1)−Co(3) | 2.519(2) | Co(3)−Co(4) | 2.705(2) |
| Te(1)−Co(4) | 2.621(2) | Co(4)−Co(4a) | 2.459(2) |
| Te(1)−Co(5) | 2.636(2) | Co(4)−Co(5) | 2.555(2) |
| Te(1)−Co(6) | 2.715(2) | Co(5)−Co(5a) | 2.529(2) |
| Te(2)−Co(2) | 2.465(2) | Co(5)−Co(6) | 2.541(2) |
| Te(2)−Co(6) | 2.595(2) | Co(6)−Co(6a) | 2.495(2) |
| Te(3)−Co(2) | 2.504(2) | Co(2)−C(1) | 1.772(11) |
| Te(3)−Co(3) | 2.510(2) | Co(3)−C(2) | 1.775(11) |
| Te(4)−Co(1) | 3.469(2) | Co(4)−C(3) | 1.774(11) |
| Te(4)−Co(3) | 2.470(2) | Co(4)−C(4) | 1.940(9) |
| Te(4)−Co(4) | 2.553(2) | Co(4)−C(5) | 2.631(14) |
| Co(1)−Co(2) | 2.531(2) | Co(5)−C(5) | 1.737(12) |
| Co(1)−Co(2a) | 2.531(2) | Co(5)−C(6) | 1.926(9) |
| Co(1)−Co(3) | 2.554(2) | Co(5)−C(7) | 1.804(12) |
| Co(1)−Co(4) | 2.564(2) | Co(6)−C(7) | 2.268(12) |
| Co(1)−Co(5) | 2.547(2) | Co(6)−C(8) | 1.949(10) |
| Co(1)−Co(6) | 2.594(2) | Co(6)−C(9) | 1.791(10) |
| Co(2)−Co(2a) | 2.610(2) | Nb(1)−C(11) | 2.046(14) |
| Co(2)−Co(3) | 2.560(2) | Nb(1)−C(10) | 2.066(14) |

| | | | |
|---|---|---|---|
| Co(5)−Te(1)−Co(6) | 56.7(1) | Te(1)−Co(4)−Te(4) | 112.4(1) |
| Co(1)−Te(1)−Co(2) | 58.7(1) | Te(1)−Co(6)−Te(2) | 111.3(1) |
| Co(2)−Te(1)−Co(3) | 60.9(1) | Co(2)−C(1)−O(1) | 179.3(8) |
| Co(2)−Te(1)−Co(4) | 110.3(1) | Co(3)−C(2)−O(2) | 178.5(9) |
| Co(2)−Te(2)−Co(6) | 64.4(1) | Co(4)−C(3)−O(3) | 177.0(10) |
| Co(2)−Te(3)−Co(3) | 61.4(1) | Co(4)−C(4)−O(4) | 139.9(3) |
| Co(3)−Te(4)−Co(4) | 65.2(1) | Co(4)−C(5)−O(5) | 124.5(9) |
| Te(1)−Co(1)−Te(1a) | 176.9(1) | Co(5)−C(5)−O(5) | 167.4(12) |
| Te(1)−Co(1)−Te(4) | 88.6(1) | Co(5)−C(6)−O(6) | 139.0(3) |
| Te(1)−Co(2)−Te(2) | 122.9(1) | Co(5)−C(7)−O(7) | 154.1(10) |
| Te(2)−Co(2)−Te(3) | 107.2(1) | Co(6)−C(7)−O(7) | 129.7(9) |
| Te(1)−Co(2)−Te(3) | 118.7(1) | Co(6)−C(8)−O(8) | 140.1(2) |
| Te(1)−Co(3)−Te(3) | 119.0(1) | Co(6)−C(9)−O(9) | 178.7(7) |
| Te(1)−Co(3)−Te(4) | 119.0(1) | C(10)−Nb(1)−C(11) | 86.3(6) |
| Te(3)−Co(3)−Te(4) | 110.0(1) | | |

established that reduction or oxidation of the cluster core of $[\mathbf{1}]^-$ by one electron or increase of the valence electron count, as in $[\mathbf{3}]^-$, only slightly affects the bonding situation within the cluster core.[4,7]

The solid-state structure of $[Cp^*_2Nb(CO)_2]$**[3]** is composed of layers containing ribbons of anions and cations parallel

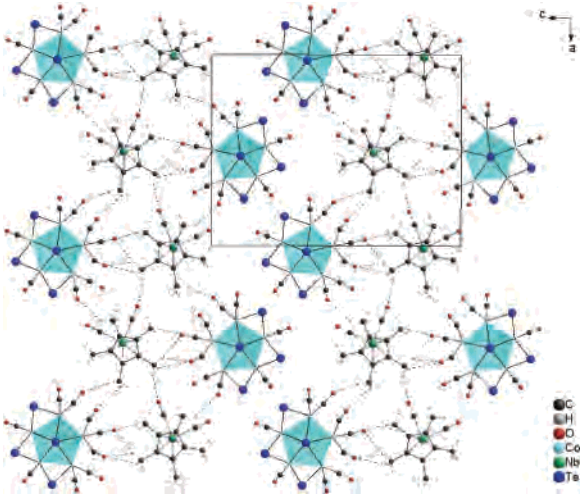


**Figure 3.** Part of the solid-state structure of $[Cp^*_2Nb(CO)_2][\mathbf{3}]$. $[Cp^*_2Nb(CO)_2]^+$ cations form zigzag chains within one sheet in the *ac* plane. The $[\mathbf{3}]^-$ anions (blue polyhedra) are associated with the cationic backbone through their CO-bridged hemispheres. CO···$CH_3$ contacts are shown between 2.540 and 2.859 Å. The next sheets below and above are displaced by *c*/2 with respect to the shown one.

to the *ac* plane. Each ribbon is built up of one-dimensional zigzag chains of $[Cp^*_2Nb(CO)_2]^+$ cations serving as a backbone to which the $Co_{10}$ prisms are associated via their CO-bridged hemisphere (Figure 3). The edges of the resulting ribbons are defined by the $\mu_4$-Te bridged faces of the prisms, which seem to be inaccessible for attractive interactions with the cations. The cationic backbone of the ribbons is mainly composed of CO···$CH_3$ interactions between methyl groups of the niobocene cation and CO bridges of the anionic cluster and, to a lesser extent, weak hydrogen bonds between neighboring cations. The range of these contacts is between 2.540 and 2.859 Å. Similar anionic−cationic interactions are also observed between the layers, and they may be responsible for the displacement of the second sheet by *c*/2 with respect to the first one.

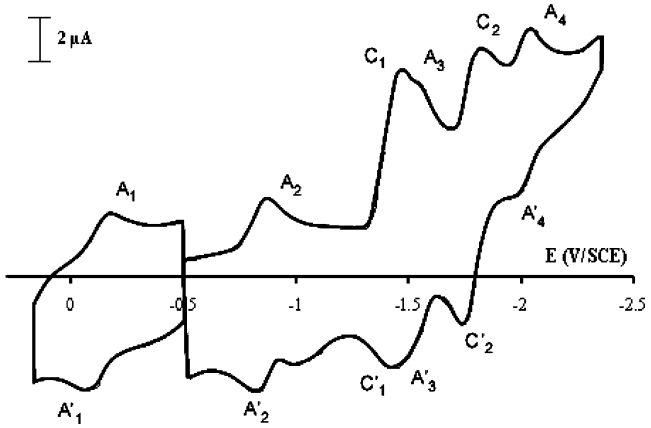


**Figure 4.** Cyclic voltammograms of $[Cp^*_2Nb(CO)_2]$[**3**] on platinum electrode in THF containing 0.2 mol/L of $NBu_4PF_6$ (scan rate = 100 mV/s).

The construction of extended arrays through the self-assembly of metal clusters by means of intermolecular hydrogen bonding between coordinated ligands is a subject of current interest.[15] The importance of hydrogen-bonding acceptor CO ligands for the crystal packing has already been discussed.[16] While there are plenty of examples for supramolecular networks comprising the bis(triphenylphosphoranylidene)ammonium cation $[Ph_3PNPPh_3]^+$,[17] examples comprising large organometallic cations like $[Cp^*_2Nb(CO)_2]^+$ are rare.

**Electrochemical Investigations.** The electron-sponge properties of the $[Co_{11}Te_7(CO)_{10}]^-$ cluster anion are already well established.[4,5] The electrochemical properties of $[Cp^*_2Nb(CO)_2][Co_{11}Te_5(CO)_{15}]$ have been investigated using cyclic voltammetry, rotating disk electrolysis (RDE), and electrolysis methods.

Cyclic voltammetry of a THF solution of $[Cp^*_2Nb(CO)_2]$-**[3]** exhibits systems $A_1/A'_1$, $A_2/A'_2$, $C_1/C'_1$, $A_3/A'_3$, $C_2/C'_2$, and $A_4/A'_4$ at −0.16, −0.80, −1.40, −1.50, −1.74, and −1.98 V, respectively (Figure 4). The system $A_1/A'_1$ corresponds to the redox reaction $[\mathbf{3}]^- + e^- \leftrightarrow [\mathbf{3}]^{2-}$. As reported elsewhere,[4] systems $C_1/C'_1$ and $C_2/C'_2$ correspond to the reduction of the cation $[Cp^*_2Nb(CO)_2]^+$, while systems $A_2/A'_2$, $A_3/A'_3$, and $A_4/A'_4$ may be attributed to three successive electron-transfer processes that finally lead to the 154-MVE pentaanion $[\mathbf{3}]^{5-}$ (eq 1).

$$[\mathbf{3}]^{2-} \underset{A_2/A'_2}{\overset{-0.80\ V}{\rightleftharpoons}} [\mathbf{3}]^{3-} \underset{A_3/A'_3}{\overset{-1.50\ V}{\rightleftharpoons}} [\mathbf{3}]^{4-} \underset{A_4/A'_4}{\overset{-1.98\ V}{\rightleftharpoons}} [\mathbf{3}]^{5-} \qquad (1)$$

Because the intensity of the oxidation peak $A'_4$ is weak, we suggest, according to our previous studies,[4] that the pentaanion generated at the potential of peak $A_4$ diffuses from the electrode toward the bulk of the solution and reduces the cation $[Cp^*_2Nb(CO)_2]^+$, which also diffuses toward the electrode (eq 2). As the pentaanion is partially consumed, its oxidation peak decreases. This reaction is thermodynamically favorable, and the neutral species "$Cp^*_2Nb(CO)_2$" may be reoxidized at the potential of peak $C'_1$.

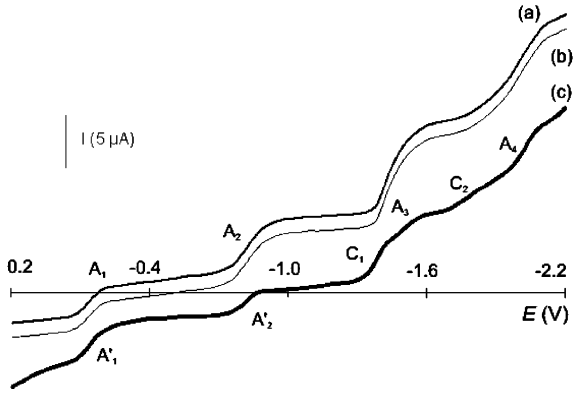


**Figure 5.** RDE voltammogram in THF of a mixture containing $[\mathbf{3}]^-$ and $[\mathbf{3}]^{2-}$ in an approximate ratio of 25:75: (a) initial product, (b) after 2 h, and (c) after electrolysis at −1 V ($n$ = 1 F).

$$[\mathbf{3}]^{5-} + [Cp^*_2Nb(CO)_2]^+ \rightarrow [\mathbf{3}]^{4-} + Cp^*_2Nb(CO)_2 \quad (2)$$

Rotating disk electrode voltammograms of solutions of $[Cp^*_2Nb(CO)_2]$**[3]** in THF revealed that a slow evolution of $[\mathbf{3}]^-$ into the dianion $[\mathbf{3}]^{2-}$ occurs without electrolysis, that is, a solution of $[\mathbf{3}]^-/[\mathbf{3}]^{2-}$ in an 81:19 ratio converts after 5 h into a 29:71 mixture. This strange phenomenon is currently under further investigation. Since the sum of the heights of reduction wave of monoanion and oxidation wave of dianion remains constant during the evolution, a disproportionation reaction may be excluded. In another experiment (Figure 5), a mixture of monoanion/dianion in an approximate ratio of 25:75 (oxidation wave $A'_1$ and reduction waves $A_1$, $A_2$, $C_1$, $A_3$, $C_2$, and $A_4$) has been converted after 2 h evolution under argon quantitatively into the dianion (oxidation wave $A'_1$). When an electrolysis is performed at −1 V (plateau of wave $A_2$) and after consumption of 1 F, the trianion is formed which upon oxidation gives waves $A'_2$ and $A'_1$. This trianion is relatively stable since no evolution of the RDE voltammogram occurs after 1 h.

**Electronic Structures of $[1]^n$ and $[3]^n$.** The electron-sponge property afforded by some transition-metal clusters is related to the existence of a range of allowed electron counts for a given architecture, that is, varying the number of electrons within this range does not significantly modify the molecular structure and connectivity. The range upper limit is usually well defined and corresponds to an electron count which satisfies the closed-shell principle. In other words, it is associated with a significant HOMO/LUMO gap separating the occupied bonding and nonbonding MO's from the vacant antibonding ones. In the case of simple molecules and for a given molecular structure, electron counts lower than this "ideal" stability count lead to first- or second-order Jahn−Teller distortion and consequently are associated with different molecular architectures. However, in the case of high-connectivity compact clusters, as well as for solid-state compounds, the Jahn−Teller instability is precluded by the connectivity. In other words, the stabilization energy which

(15) (a) Roland, B. K.; Selby, H. D.; Cole, J. R.; Zheng, Z. *Dalton Trans.* **2003**, 4307−4312. (b) Fujimura, T.; Seino, H.; Hidai, M.; Mizobe, Y. *J. Organomet. Chem.* **2004**, *689*, 738−743.
(16) (a) Braga, D.; Grepioni, F.; Desiraju, G. R. *J. Organomet. Chem.* **1997**, *548*, 33−43. (b) Desiraju, G. R. *J. Chem. Soc., Dalton Trans.* **2000**, 3745−3751.
(17) Lewis, G. R.; Dance, I. *J. Chem. Soc., Dalton Trans.* **2000**, 299−306.

**Table 2.** Optimized Geometries and HOMO/LUMO Gaps for $Ni_{10}$ and $M_{11}$ (M = Ni, Co) Clusters[a]

| | | | | M−M distances (Å) | | | | | |
|---|---|---|---|---|---|---|---|---|---|
| | MVE | geometry | HOMO/LUMO gap (eV) | intra-pentagonal | | inter-pentagonal | | center to vertex | |
| | | | $Ni_{10}$ clusters | | | | | | |
| $[Ni_{10}(PMe)_7(CO)_{10}]^{2-}$ | 150 | PP ($D_{5h}$) | 0.46 | (2.62)[8] | 2.542 | (2.610)[8] | 2.649 | | |
| $[Ni_{10}Te_7(CO)_{10}]^{2-}$ | 150 | PP ($D_{5h}$) | 0.40 | | 2.673 | | 2.687 | | |
| $[Ni_{10}Te_7(CO)_{10}]^{2+}$ | 146 | PP ($D_{5h}$) | 0.20 | | 2.676 | | 2.471 | | |
| $[Ni_{10}Te_2(CO)_{20}]^{2+}$ | 146 | PP ($D_{5h}$) | 0.21 | | 2.701 | | 2.566 | | |
| $[Ni_{10}Te_2(CO)_{20}]^{2+}$ | 146 | PA ($D_{5d}$) | 1.01 | | 2.716 | | 2.516 | | |
| $[Ni_{10}Te_2(CO)_{20}]^{2-}$ | 150 | PP ($D_{5h}$) | 0.51 | | 2.700 | | 2.553 | | |
| $[Ni_{10}Te_2(CO)_{20}]^{2-}$ | 150 | PA ($D_{5d}$) | 0.14 | | 2.673 | | 2.687 | | |
| $[Ni_{10}(PMe)_2(CO)_{18}]^{2-}$ | 146 | PA ($C_{2h}$) | 1.76 | (2.61)[22] | 2.633 | (2.490) | 2.507 | | |
| $[Ni_{10}(AsMe)_2(CO)_{18}]^{2-}$ | 146 | PA ($C_{2h}$) | 1.66 | (2.68)[22] | 2.700 | (2.490) | 2.517 | | |
| $[Ni_{10}(SbMe)_2(CO)_{18}]^{2-}$ | 146 | PA ($C_{2h}$) | 1.47 | (2.80)[22] | 2.815 | (2.496) | 2.510 | | |
| $[Ni_{10}(BiMe)_2(CO)_{18}]^{2-}$ | 146 | PA ($C_{2h}$) | 1.37 | (2.87)[22] | 2.881 | (2.505) | 2.547 | | |
| $[Ni_{10}(\mu_{10}\text{-Ge})(CO)_{20}]^{2-}$ | 146 | PA ($D_{5d}$) | 1.54 | (2.54)[23] | 2.596 | (2.721) | 2.706 | 2.470 | 2.480 |
| | | | metal-centered $M_{11}$ clusters | | | | | | |
| $[Ni_{11}(Bi)_2(CO)_{18}]^{2-}$ | 154 | PA ($C_{2h}$) | 0.43 | (2.81)[25] | 2.786 | (2.51) | 2.514 | (2.59) | 2.578 |
| $[Ni_{11}(Bi)_2(CO)_{20}]$ | 156 | PA ($D_{5d}$) | 0.56 | | 2.786 | | 2.514 | | 2.578 |
| $[Ni_{11}(Sb)_2(CO)_{18}]^{2-}$ | 154 | PA ($C_{2h}$) | 0.58 | (2.77)[27] | 2.756 | (2.49) | 2.510 | (2.57) | 2.561 |
| $[Ni_{11}(Se)_2(CO)_{18}]^{2-}$ | 156 | PA ($C_{2h}$) | 0.66 | (2.74)[24] | 2.745 | (2.52) | 2.554 | (2.57) | 2.561 |
| $[Ni_{11}(SnR)_2(CO)_{18}]^{2-}$ | 154 | PA ($C_{2h}$) | 0.23 | (2.79)[26] | 2.783 | (2.51) | 2.547 | (2.58) | 2.593 |
| $[Ni_{11}(Te)_2(CO)_{20}]^{2+}$ | 156 | PP ($D_{5h}$) | 0.72 | (2.81) | 2.784 | (2.51) | 2.550 | (2.59) | 2.585 |
| $[Ni_{11}(Te)_2(CO)_{18}]^{2-}$ | 156 | PA ($C_{2h}$) | 1.62 | (2.81) | 2.791 | (2.51) | 2.543 | (2.59) | 2.588 |
| $[Ni_{11}(Te)_2(CO)_{18}]^{2+}$ | 152 | PA ($C_{2h}$) | 0.10 | | 2.810 | | 2.557 | | 2.592 |
| $[Ni_{11}(Te)_2(CO)_{18}]^{2+}$ | 152 | PP ($D_{5h}$) | 0.25 | | 2.655 | | 2.656 | | 2.653 |
| $[Co_{11}(Te)_5(CO)_{15}]^{5-}$ | 154 | PP ($C_{2v}$) | 0.06 | | 2.658 | | 2.546 | | 2.543 |
| $[Co_{11}(Te)_2(CO)_{18}]^{3-}$ | 146 | PA ($C_{2h}$) | 0.07 | | 2.592 | | 2.520 | | 2.475 |
| $[Ni_{11}Te_7(CO)_{10}]^{2-}$ | 160 | PP ($D_{5h}$) | 0.15 | | 2.698 | | 2.497 | | 2.534 |

[a] Available experimental distances are given in parentheses. PP and PA are $D_{5h}$ pentagonal-prismatic, $D_{5d}$ and $C_{2h}$ pentagonal-antiprismatic geometries, respectively.

would be gained upon the expected Jahn−Teller distortion is overcome by the destabilization energy which would arise from the weakening of too many spectator bonds. Consequently, electron counts lower than that satisfying the closed-shell requirement become possible for the same architecture. Such a situation has been clearly shown for hexacapped cubic transition-metal clusters for example.[18] Thus, from the point of view of bonding, it is important to determine first the electron count which allows an electron-sponge system to satisfy the closed-shell principle.

Since the rather low symmetry of the $[Co_{11}Te_5(CO)_{15}]^n$ system renders its orbital analysis more difficult, we have investigated in a previous step the related but more symmetrical $[Co_{11}Te_7(CO)_{10}]^n$, **[1]**$^n$ ($n = 0, -1, -2$) series.[4,7,19] The bonding in a centered cluster is usually better understood as deriving from the interaction between the interstitial atom and the cluster host cage.[18,20] Thus, we start our analysis by investigating empty $M_{10}$ pentagonal prismatic (PP) clusters. For such a moderately compact architecture exhibiting 15 M−M contacts, the 18-electron rule is likely to be satisfied, that is, a closed-shell electron count of $18 \times 10 - 2 \times 15 = 150$ metal valence electrons (MVE) is expected. Indeed, this is the count of $[Ni_{10}(PMe)_7(CO)_{10}]^{2-}$ which depicts a metallic PP cage with all its faces capped by PMe ligands.[8] As a matter of fact, DFT calculations carried out on the $[Ni_{10}(PMe)_7(CO)_{10}]^{2-}$ and $[Ni_{10}Te_7(CO)_{10}]^{2-}$ models (150 MVE's) assuming the $D_{5h}$ PP structure gave optimized geometries (Table 2) with moderate but significant HOMO/LUMO gaps (0.46 and 0.40 eV, respectively).

The addition of a supplementary metal at the center of the $D_{5h}$ pentagonal prism induces orbital interactions which cannot be described within the localized 2-electron/2-center bonding scheme upon which the 18-electron rule is based. Indeed, the encapsulated metal atom has only 9 valence atomic orbitals (AOs) to ensure 10 M−M contacts. Moreover, if its s and p valence AOs are expected to interact with the PP cage, it is less straightforward for the more contracted d AOs. All, part of, or none of them could a priori lead to significant interaction with the host cage.[18] Calculations show that only the $d_{z^2}$ AO of the central atom does not interact and leads to an essentially nonbonding MO of $a'_1$ symmetry, as illustrated in the sketch on the left-hand-side of Figure 6. Indeed, this orbital points toward the centers of the large pentagonal faces of the $Co_{10}$ prism where there is no electron density. The nonbonding character of this $a'_1(z^2)$ MO has also been pointed out in previous calculations.[4] Thus, the closed-shell principle requires the occupation of this essentially nonbonding $a'_1(z^2)$ MO for such an $M_{11}$ architecture, leading to its largest possible electron count of 152 MVE's. This does not mean that the highly negatively charged 152-MVE **[1]**$^{5-}$ anion should be characterized, but at least some related 152-MVE compounds exhibiting the same PP architecture should be stable and exhibit a diamagnetic behavior.[5]

(18) (a) Halet, J.-F.; Saillard, J.-Y. *Struct. Bonding* **1997**, *87*, 81−109. (b) Gautier, R.; Halet, J.-F.; Saillard, J.-Y. In *Metal Clusters in Chemistry*, Vol. 3; Braunstein, P., Oro, L. A., Raithby, P. R., Eds.; Wiley-VCH: Weinheim, Germany, 1999; pp 1643−1663 and references therein.
(19) Brunner, H.; Ebner, A.; Wachter, J.; Zabel, M. *C. R. Chim.* **2005**, *8*, 1856−1862.
(20) Mingos, D. M. P.; Wales, D. J. *Introduction to Cluster Chemistry;* Prentice Hall: Edgewood Cliffs, NJ, 1990.

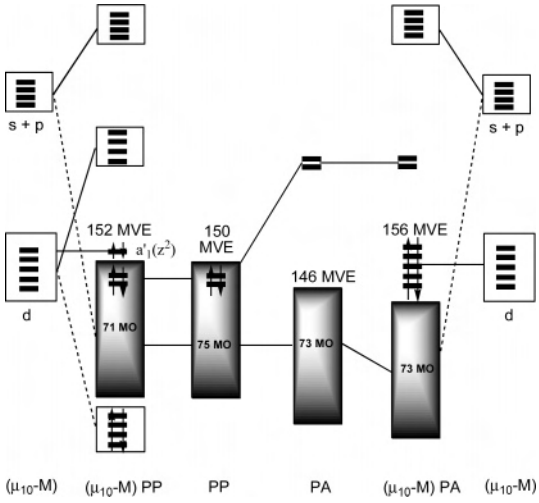


**Figure 6.** MO diagrams illustrating the closed-shell requirement for noncentered ($M_{10}$) and centered ($M_{11}$) pentagonal-prismatic (PP) and pentagonal-antiprismatic (PA) model clusters.

The computed MO diagrams of the ground states of the 146, 147, 148, 149, 150, and 152-MVE **[1]**$^n$ ($n$ = +1, 0, −1, −2, −3, −5) species are shown in Figure 7. Pertinent optimized data are given in Table 3. The closed-shell configuration of the 152-MVE species is secured by a moderate but significant HOMO−LUMO gap of 0.49 eV. A decrease of the electron count corresponds to the depopulation of the $14e''_2$ and $15a'_1$ orbitals. The latter is the nonbonding $d_{z^2}$ AO of the central atom discussed above. There is a good agreement between the optimized and experimental distances in the 148- and 149-MVE clusters (Table 3). It is noteworthy that the 148- and 150-MVE species exhibit singlet and triplet states lying very close in energy. Such a situation of near spin-state degeneracy is not uncommon for clusters which are electron deficient with respect to the closed-shell principle.[18]

The related but less symmetrical ($C_{2v}$) 150-, 151-, and 152-MVE $[Co_{11}Te_5(CO)_{15}]^n$ (**[3]**$^n$) ($n$ = −1, −2, −3) series exhibits an electronic structure similar to that of the related **[1]**$^n$ species (Table 4 and Figure 8). In particular, one can note the nonbonding character of the $d_{z^2}$ orbital of the encapsulated atom (MO $51a_1$) and the existence of a significant HOMO/LUMO gap achieving the fulfilment of the closed-shell principle for the 152-MVE count. As for the **[1]**$^n$ series, there is a good agreement between the optimized and available experimental distances (Table 4). Interestingly, the 150-MVE species shows nearly degenerate singlet and triplet states with the electron configurations depicted in Figure 7.

The fact that the stable anion **[3]**$^-$ can be electrochemically reduced to **[3]**$^{5-}$ through four reversible one-electron transfers is at first sight puzzling since the tetra- and pentaanions exceed the PP closed-shell 152-MVE count by 1 and 2 electrons, respectively. One possible explanation is that skeletal distortion away from the ideal PP architecture occurs, thus leading to a new structure associated with another closed-shell electron count. To check this hypothesis, the structure of **[3]**$^{5-}$ has been optimized. The lowest energy was found for a singlet state having a structure of $C_s$ symmetry. This structure derives from the regular PP arrangement by significant elongation of two Co−Co edges on each $Co_5$ pentagon, both elongated edges being eclipsed (Figure 9). The corresponding Co−Co distance (2.974 Å) is merely bonding, even considering that calculating highly charged anion in vacuum tends to overestimate bond distances. With a HOMO/LUMO gap of 0.36 eV, the closed-shell principle can be considered fulfilled for the count of 154 MVE's.

**Magnetic Behavior of [1]$^-$.** To test our theoretical predictions on the electron configuration of the title cobalt clusters, we have been able to prepare a stable powdered sample of analytically pure $[Cp^*_2Nb(CO)_2][Co_{11}Te_7(CO)_{10}]$ upon which we have carried out magnetization measurements. The results obtained allow us to identify the magnetic nature of the ground state of the cluster anion **[1]**$^-$. At room temperature, the sample is paramagnetic with an effective magnetic moment, $\mu_{eff}$ = 2.65 $\mu_B$, slightly smaller than expected for a triplet state ($S$ = 1) with a free-electron Zeeman factor ($g$ = 2.00, $\mu_{eff}$ = 2.83 $\mu_B$). When cooled, the magnetic susceptibility passes through a broad maximum at $T_{max}$ = 100 K which is a clear signature of the presence of a nonmagnetic ground state with a thermally populated magnetic excited state (Figure 10).[21] The energy gap, $J$, between the ground and the first excited is estimated from the Boltzmann population of the triplet state which splits under the action of the external magnetic field. $J$ is related to $T_{max}$ through the simple expression $J/kT_{max}$ = 1.6, $k$ being the Boltzmann constant in wavenumber per kelvin.[21] The singlet−triplet gap is then equal to 0.318 kcal/mol, a very small value. This result is in a rather good qualitative agreement with the DFT calculations which found the ground state to be a triplet, but with a triplet-singlet separation of ∼2 kcal/mol, a value not significantly different from zero at the considered level of theory and which is on the order of magnitude of the electrostatic effects present in the crystal and not considered in the calculations.

**Related Structures and Compounds.** At this point of the analysis, comparison between the pentagonal prismatic (PP) and pentagonal antiprismatic (PA) structures is appealing. PA cages are also called icosahedral *arachno* structures since they derive from the icosahedron by removal of two opposite vertices. Because of their high connectivity, localized bonding schemes such as the 18-electron rule do not apply properly. The more appropriate polyhedral skeletal electron-pair (PSEP) theory[20] for this kind of species predicts a closed-shell count of 146 MVE's for PA $M_{10}$ clusters. This is in fact the count of the diamagnetic arachno $[Ni_{10}(EMe)_2(CO)_{18}]^{2-}$ (E = P, As, Sb, Bi) series.[22] Thus, for an $M_{10}$ cluster, the PP → PA structural change induces the transformation of two nonbonding orbitals into two antibonding ones, as sketched in the middle of Figure 6. This PP versus PA structural preference with respect to the electron count is nicely illustrated by our results on the 146-MVE $[Ni_{10}Te_2$-

(21) Kahn, O. *Molecular Magnetism*; VCH: New York, 1993.
(22) (a) Rieck, D. F.; Montag, R. A.; McKechnie, T. S.; Dahl, L. F. *J. Chem. Soc., Chem. Commun.* **1986**, 1330−1331. (b) Mlynek, P. D.; Dahl, L. F. *Organometallics* **1997**, *16*, 1655−1667.

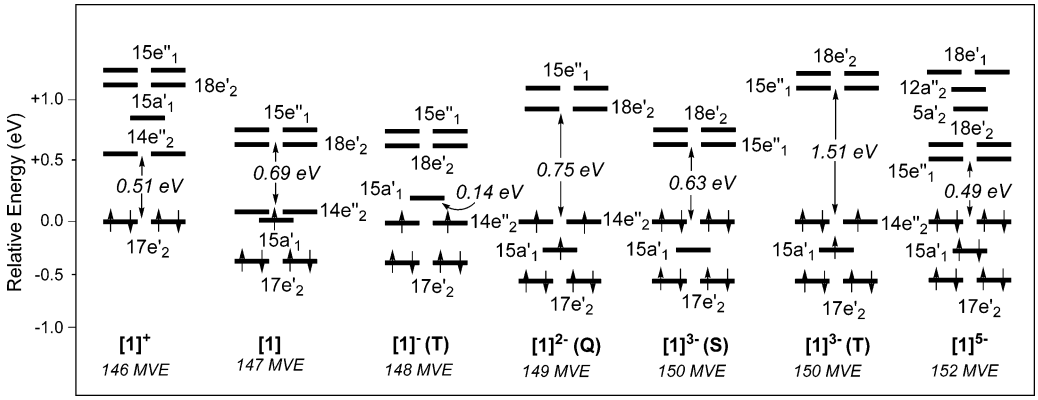


**Figure 7.** Frontier MO diagram of the $[Co_{11}Te_7(CO)_{10}]^n$ ([**1**]$^n$, $n = +1, 0, -1, -2, -3, -5$) series.

**Table 3.** Optimized Geometries of the PP $[Co_{11}Te_7(CO)_{10}]^n$ ([**1**]$^n$, $n = 0, +1, -1, -2, -3, -4, -5$) Clusters[a]

| $n$ | +1 | 0 | −1 | | −2 | −3 | | −4 | −5 |
|---|---|---|---|---|---|---|---|---|---|
| MVE | 146 | 147 | 148 | | 149 | 150 | | 151 | 152 |
| spin state | singlet | singlet | triplet | singlet | quadruplet | triplet | singlet | doublet | singlet |
| bond distances | | | | | | | | | |
| Co−Co$_{intrapent}$ | 2.542 | 2.542 (2.57)[19] | 2.596 | 2.508 (2.58)[4] | 2.579 (2.567)[6] | 2.606 | 2.641 | 2.648 | 2.648 |
| Co−Co$_{interpent}$ | 2.572 | 2.572 (2.61) | 2.590 | 2.617 (2.61) | 2.622 (2.622) | 2.627 | 2.682 | 2.633 | 2.633 |
| Co$_{central}$−Co | 2.515 | 2.515 (2.55) | 2.562 | 2.503 (2.56) | 2.556 (2.534) | 2.576 | 2.616 | 2.609 | 2.609 |
| Co−($\mu_5$-Te) | 2.522 | 2.522 (2.58) | 2.536 | 2.560 (2.57) | 2.555 (2.562) | 2.556 | 2.590 | 2.553 | 2.553 |
| Co−($\mu_4$-Te) | 2.506 | 2.506 (2.52) | 2.496 | 2.517 (2.50) | 2.502 (2.510) | 2.500 | 2.496 | 2.493 | 2.493 |
| Co$_{central}$−($\mu_4$-Te) | 3.485 | 3.478 (3.49) | 3.478 | 3.477 (3.49) | 3.472 (3.470) | 3.475 | 3.474 | 3.493 | 3.480 |
| Co$_{central}$−($\mu_5$-Te) | 2.585 | 2.663 (2.68) | 2.543 | 2.543 (2.542) | 2.612 (2.642) | 2.519 | 2.630 | 2.609 | 2.517 |
| Co−C | 1.702 | 1.739 (1.78) | 1.729 | 1.729 (1.74) | 1.721 (1.760) | 1.717 | 1.708 | 1.721 | 1.720 |
| relative energy (kcal/mol) | | | 0.0 | +2.1 | | 0.0 | +1.6 | | |

[a] Relative energies refer to the singlet/triplet separation. Available experimental distances are given in parenthesis.

**Table 4.** Optimized Geometries of the PP $[Co_{11}Te_5(CO)_{15}]^n$ ([**3**]$^n$; $n = -1, -2, -3, -5$) Clusters[a]

| $n$ | −1 | | −2 | −3 | −5 |
|---|---|---|---|---|---|
| MVE | 150 | | 151 | 152 | 154 |
| spin state | triplet | singlet | doublet | singlet | singlet |
| symmetry | $C_{2v}$ | $C_{2v}$ | $C_{2v}$ | $C_{2v}$ | $C_s$ |
| bond distances | | | | | |
| Co−Co$_{intrapent}$ | 2.637 | 2.618 (2.64) | 2.627 | 2.579 | 2.797 (av) |
| Co−Co$_{interpent}$ | 2.524 | 2.553 (2.53) | 2.528 | 2.622 | 2.616 (av) |
| Co$_{central}$−Co | 2.606 | 2.586 (2.57) | 2.547 | 2.556 | 2.673 (av) |
| Co−($\mu_5$-Te) | 2.545 | 2.576 (2.56) | 2.485 | 2.555 | 2.661 (av) |
| Co−($\mu_4$-Te) | 2.476 | 2.496 (2.52) | 2.487 | 2.502 | 2.531 (av) |
| Co$_{central}$−($\mu_5$-Te) | 2.614 | 2.614 (2.62) | 2.622 | 2.619 | 2.596 (av) |
| Co−C | 1.725 | 1.729 (1.75) | 1.729 | 1.721 | 1.722 (av) |
| relative energy (kcal/mol) | +1.3 | 0.00 | | | |

[a] Relative energies refer to the singlet/triplet separation. Experimental distances (from this work) are given in parentheses.

$(CO)_{20}]^{2+}$ and 150-MVE $[Ni_{10}Te_2(CO)_{20}]^{2-}$ models, which have been optimized assuming both PP ($D_{5h}$) and PA ($D_{5d}$) structures (Table 2). The former is found to be more stable by 12.2 kcal/mol and to have a large HOMO/LUMO gap in the PA arrangement, whereas the latter is more stable by 15.3 kcal/mol in the PP arrangement, with a larger HOMO/LUMO gap.

A 146-MVE germanium-centered decanuclear PA cluster, namely, $[Ni_{10}(\mu_{10}\text{-Ge})(CO)_{20}]^{2-}$, has been characterized.[23] It also obeys the usual PSEP electron counting rules for centered clusters in that in this compound all the 4s and 4p Ge AO's participate to the bonding. Several examples of metal-centered PA nickel clusters are also known: $[Ni_{11}Se_2(CO)_{18}]^{2-}$ (156 MVE's),[24] $[Ni_{11}Bi_2(CO)_{18}]^{2-/3-}$ (154/155 MVE's),[25] $[Ni_{11}SnR_2(CO)_{18}]^{2-}$ (R = *n*-Bu, Me; 154 MVE's),[26] $[Ni_{11}Sb_2(CO)_{18}]^{2-/3-}$ (154/155 MVE's),[27] and $[Ni_{11}\{SbNi(CO)_3\}_2(CO)_{18}]^{2-/3-/4-}$ (154/155/156 MVE's).[28] In this series, the closed-shell electron count is 156 MVE's.[28b] This indicates that in these compounds the five 3d AO's of the encapsulated Ni atom do not interact significantly with the hosting cage.[26] Such a situation is sketched on the right-hand-side of Figure 6. Consequently, their occupation is necessary to fulfill the closed-shell requirement. Our calculations on various noncentered and centered PA nickel clusters confirm that the closed-shell requirement is satisfied for 146, 146, and 156 MVE's in the case of noncentered, Ge-centered, and Ni-centered species, respectively (Table 2). Indeed, substantial HOMO−LUMO gaps separating nonbonding

(23) Ceriotti, A.; Demartin, F.; Heaton, B. T.; Ingallina, P.; Longoni, G.; Manassero, M.; Marchionna, M.; Masciocchi, N. *J. Chem. Soc., Chem. Commun.* **1989**, 786−787.
(24) Kahaian, A. J.; Thoden, J. B.; Dahl, L. F. *J. Chem. Soc., Chem. Commun.* **1992**, 353−355.
(25) Albano, V. G.; Demartin, F.; Iapalucci, M. C.; Longoni, G.; Monari, M.; Zanello, P. *J. Chem. Soc., Dalton Trans.* **1992**, 497−502.
(26) Zebrowski, J. P.; Hayashi, R. K.; Dahl, L. F. *J. Am. Chem. Soc.* **1993**, *115*, 1142−1144.
(27) Albano, V. G.; Demartin, F.; Femoni, C.; Iapalucci, M. C.; Longoni, G.; Monari, M.; Zanello, P. *J. Organomet. Chem.* **2000**, *593*−*594*, 325−334.
(28) (a) Albano, V. G.; Demartin, F.; Iapalucci, M. C.; Lashi, F.; Longoni, G.; Sironi, A.; Zanotti, V. *J. Chem. Soc., Chem. Commun.* **1990**, 547−548. (b) Albano, V. G.; Demartin, F.; Iapalucci, M. C.; Lashi, F.; Longoni, G.; Sironi, A.; Zanello, P. *J. Chem. Soc., Dalton Trans.* **1991**, 739−748.

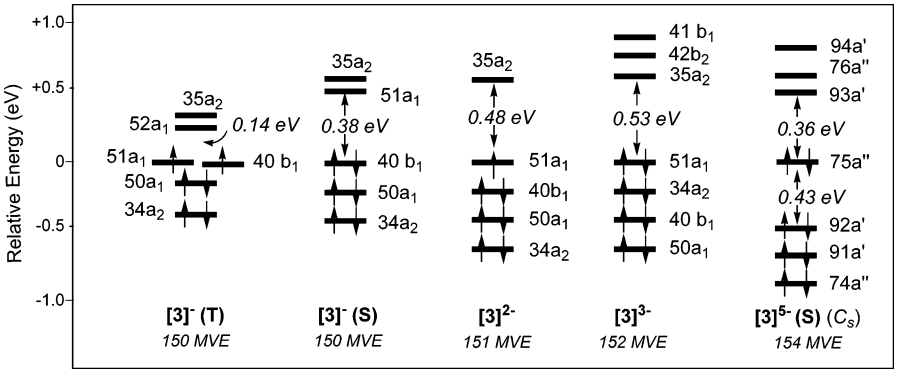


**Figure 8.** Frontier MO diagram of the $[Co_{11}Te_5(CO)_{15}]^n$ ([**3**]$^n$, $n = -1, -2, -3, -5$) series.

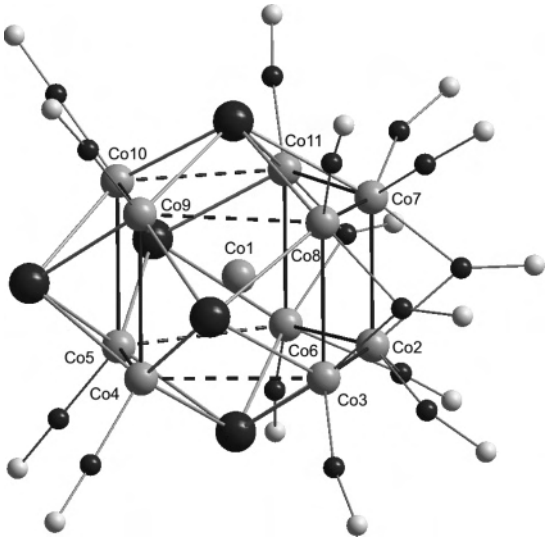


**Figure 9.** Optimized structure of the 154-MVE anion [**3**]$^{5-}$ of $C_s$ symmetry. The dashed lines indicate the elongated Co−Co distances (2.975 Å).

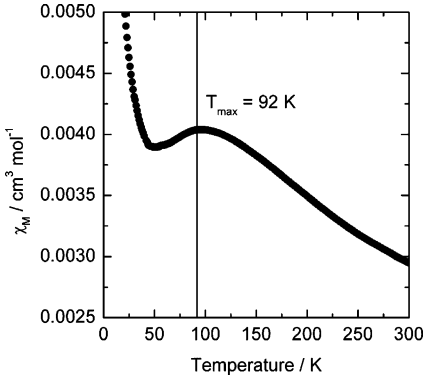


**Figure 10.** Variation of the magnetic susceptibility of $[Cp^*_2Nb(CO)_2]$-$[Co_{11}Te_7(CO)_{10}]$ with temperature.

HOMO's from antibonding LUMO's are found for these particular electron counts. It is worth mentioning that the available X-ray data are in good agreement with our optimized molecular structures.

## Conclusions

In conclusion, a novel anionic hybrid carbonyl-telluride cobalt cluster belonging to the rare type of pentagonal-prismatic $M_{10}$ polyhedral geometry is described. Although the yield is modest, its importance lies in that it extends the electron configuration of the known metal-centered $Co_{11}$ clusters from 147 ([**1**]$^0$) up to 154 MVE's ([**3**]$^{5-}$), thus giving rise to exploration of the electronic structures of differently charged clusters. The unique ligand shell of [**3**]$^-$ is composed of two $\mu_5$-Te, three $\mu_4$-Te, and 15 CO ligands in terminal, symmetrical, and semibridging bonding modes. Interactions of the CO-bridging half-shell with $[Cp^*_2Nb(CO)_2]^+$ cations gives rise to the formation of supramolecular networks containing ribbons of anions and cations. Electrochemical studies reveal the presence of four redox couples within the series of [**3**]$^n$ ($n = -1$ to $-5$) anions.

$M_{10}$ clusters depicting noncentered PP or PA architectures are likely to be stable for one single MVE count corresponding to the fulfillment of the closed-shell principle or for a very narrow range of allowed electron counts lying just below this closed-shell MVE count. These MVE counts are 150 and 146 for the PP and PA arrangements, respectively. On the other hand, because of their higher connectivity, $M_{11}$-centered PP or PA architectures allow larger ranges of electron counts, below their closed-shell MVE counts which are 152 and 156, respectively. Thus, electron counts lower than the ideal closed-shell MVE values correspond to small HOMO−LUMO gaps associated with low-lying high-spin states, as exemplified by the experimental magnetic behavior of a salt of [**1**]$^-$ for which the triplet state is found to lie 0.32 kcal/mol above the singlet state. On the other hand, electron counts larger than the ideal closed-shell MVE values are expected to lead to distortion of the regular centered PP or PA architectures, as shown theoretically for the 154 MVE's [**3**]$^{5-}$ cluster.

## Experimental Section

**General Methods.** All procedures were carried out under $N_2$ using dry solvents. Elemental analyses (C, H) were performed at the Mikroanalytisches Laboratorium, Universität Regensburg. IR spectra were obtained with a Bio Rad FT-IR FTS 3000MX spectrometer. ESI mass spectra were obtained on a ThermoQuest-Finnigan TSQ 7000 spectrometer. $Cp^*_2Nb(Te_2H)$ was prepared from $Cp^*_2NbBH_4$ and elemental tellurium.[29] Electrochemical experiments were carried out as described in reference 5.

**$[Cp^*_2Nb(CO)_2][Co_{11}Te_5(CO)_{15}]$.** A mixture of $Cp^*_2Nb(Te_2H)$ (330 mg, 0.53 mmol), $Co_2(CO)_8$ (370 mg, 1.08 mmol), and toluene

(29) Blacque, O.; Brunner, H.; Kubicki, M. M.; Nuber, B.; Stubenhofer, B.; Wachter, J.; Wrackmeyer, B. *Angew. Chem., Int. Ed. Engl.* **1997**, *36*, 351−353.

**Table 5.** Crystallographic Data for Complex $[Cp^*_2Nb(CO)_2][Co_{11}Te_5(CO)_{15}]$

| | |
|---|---|
| formula | $C_{37}H_{30}Co_{11}NbO_{17}Te_5$ |
| mol wt | 2125.75 |
| $T$ (K) | 173(1) |
| cryst size (mm) | $0.28 \times 0.02 \times 0.02$ |
| cryst syst | orthorhombic |
| space group | $P_{nma}$ |
| $a$ (Å) | 15.640(2) |
| $b$ (Å) | 16.638(2) |
| $c$ (Å) | 20.448(3) |
| $V$ (Å$^3$) | 5321(1) |
| $Z$ | 4 |
| $d_{calcd}$ (g/cm$^3$) | 2.654 |
| $\mu$ (mm$^{-1}$) | 6.287 |
| instrument | Stoe-IPDS |
| $\Theta$ (deg) | 1.99−25.74 |
| reflns collected | 62 764 |
| independent reflns | 5230 |
| $R_{int}$ | 0.155 |
| obsd reflns | 2840 ($I > 2.5\sigma$) |
| params | 343 |
| abs correction | numerical |
| $T_{max}$, $T_{min}$ | 0.771/0.907 |
| max/min residual density (e/Å$^{-3}$) | 0.754/−0.815 |
| R1, wR2 ($I > 2\sigma$) | 0.0322, 0.0779 |
| R1, wR2 (all data) | 0.0858, 0.1072 |

(150 mL) was stirred at 115 °C for 3 h. After vigorous gas evolution a dark powder precipitated, which was separated and washed several times with toluene. The black residue was dissolved in $CH_2Cl_2$ (25 mL) and chromatographed on $SiO_2$ (activity II/III; column 15 × 3 cm). Continuous elution with $CH_2Cl_2$ gave successively two broad red-brown bands containing, after removal of the solvent, $[Cp^*_2Nb(CO)_2]$[**1**] (162 mg, 14%)[5] and $[Cp^*_2Nb(CO)_2]$**[2]** (80 mg, 8%),[9] respectively. Then, with $CH_2Cl_2$/acetone (100:1) a dark brown band was eluted containing $[Cp^*_2Nb(CO)_2]$-**[3]** (67 mg, 6%with respect to $Cp^*_2NbTe_2H$). The latter compound was recrystallized from $CH_2Cl_2$/acetone (10:1).

**$[Cp^*_2Nb(CO)_2]$[3].** IR (KBr): $\nu$(CO) 2007s, 1961vs, 1820s, 1790sh cm$^{-1}$. NI-ESI-MS (from $CH_3CN$): $m/z$ 1708 ($[Co_{11}{}^{128}Te_5(CO)_{15}]^-$ = 1709). PI-ESI-MS: $m/z$ 419.0 ($[C_{20}H_{30}Nb(CO)_2]^+$). Anal. Found (calcd) for $C_{37}H_{30}Co_{11}NbO_{17}Te_5$ (2125.81): C, 21.23 (20.90); H, 2.06 (1.42).

**Crystal Structure Determination of $[Cp^*_2Nb(CO)_2]$[3]**. Crystallographic data and details of the measurements are summarized in Table 5. The structure was solved by direct methods and least-squares refinement. Program package Step 32 with SIR97 and SHELXL97 was employed using all unique reflections. Non-hydrogen atoms were refined anisotropically, and hydrogen atoms were added in calculated positions.

**Computational Details.** Density functional theory calculations were carried out using the Amsterdam Density Functional (ADF) package developed by Baerends and co-workers.[30] The results discussed in this paper were obtained assuming the local density approximation of electron correlation using the Vosko−Wilk−Nusair parametrization[31] and nonlocal density approximation assuming corrections of Becke[32] and Perdew[33] for the exchange and correlation energies, respectively. The standard TZP basis set of the ADF program[30] was used for the atoms constituting all the computed compounds. The frozen-core approximation was used to treat the core electrons.

**Magnetic Measurements.** The magnetizations have been recorded with a Quantum Design MPMS SQUID magnetometer operating in the temperature range of 2−300 K with a DC magnetic field up to 5 T. The experimental data have been corrected from the diamagnetism of the sample holder and the intrinsic diamagnetism of the materials evaluated with Pascal's tables.

**Acknowledgment.** We thank Prof. Dr. H. Brunner for support and we are grateful to the Deutsche Forschungsgemeinschaft for financial support. B.Z. is grateful to the IDB for financial support. The theoretical part of this work was supported by the French-Algerian CNRS-DEF program 17922. Computing facilities were provided by the PCIO center of the University of Rennes I and the IDRIS-CNRS center at Orsay.

**Supporting Information Available:** One X-ray crystallographic file in CIF format. This material is available free of charge via the Internet at http://pubs.acs.org.

IC061904+

(30) (a) *ADF2.3* and *ADF2002.01*; SCM, Theoretical Chemistry, Vrije Universiteit: Amsterdam, The Netherlands, http://www.scm.com. (b) Baerends, E. J.; Ellis, D. E.; Ros, P. *Chem. Phys.* **1973**, *2*, 41−51. (c) Baerends, E. J.; Ros, P. *Int. J. Quantum Chem.* **1978**, *S12*, 169−190. (d) Boerrigter, P. H.; te Velde, G.; Baerends, E. J. *Int. J. Quantum Chem.* **1988**, *33*, 87−113. (e) te Velde, G.; Baerends, E. J. *J. Comput. Phys.* **1992**, *99*, 84−98. (f) Fonseca, Guerra, C.; Snijders, J. G.; te Velde, G.; Baerends, E. J. *Theor. Chem. Acc.* **1998**, *99*, 391−403. (g) te Velde, G.; Bickelhaupt, F. M.; van Gisbergen, S. J. A.; Fonseca Guerra, C.; Baerends, E. J.; Snijders, J. G.; Ziegler, T. *J. Comput. Chem.* **2001**, *22*, 931−967.

(31) Vosko, S.; Wilk, L.; Nusair, M. *Can. J. Chem.* **1990**, *58*, 1200−1211.

(32) (a) Becke, A. D. *J. Chem. Phys.* **1886**, *84*, 4524−4529. (b) Becke, A. D. *Phys. Rev. A* **1988**, 3098−3100.

(33) (a) Perdew, J. P. *Phys. Rev. B* **1986**, *33*, 8822−8824. (b) Perdew, J. P. *Phys. Rev. B* **1986**, *34*, 7406−7406.